J Mater Sci (2006) 41:7393–7400
DOI 10.1007/s10853-006-0812-2

Processing of submicrometric $CaTi_{0.8}Fe_{0.2}O_{3-\delta}$ ceramics by mechanical activation

R. O. Fuentes · E. Chinarro · F. M. Figueiredo · R. Soares · F. M. B. Marques · J. R. Frade

Received: 8 September 2005 / Accepted: 2 December 2005 / Published online: 20 September 2006

Abstract Effects of mechanical activation of precursors in order to obtain $CaTi_{0.8}Fe_{0.2}O_{3-\delta}$ are reported. Mixtures of $CaCO_3$, TiO_2 and Fe_2O_3 were dry-grinded in Teflon or zirconia containers using planetary ball-mills at different rotations (200, 300 and 500 rpm) and for various periods of time. The perovskite is not formed just by milling and a subsequent heat treatment at 800–1,000 °C was necessary. This still represents a significant advantage over the classical ceramic route as a result of the improved reaction kinetics due to the smaller grain size (< 100 nm) of the activated powders and a modification of the thermodynamic initial state. Dense ceramic samples showing a bimodal submicrometric grain-size distribution (100–200 and 250–500 nm) were obtained after sintering the activated powders at 1,150 °C. TEM revealed homogeneous samples, free from inhomogeneities such as core-shell grains typically observed in ceramics obtained from non-activated precursors sintered at 1,320–1,350 °C.

R. O. Fuentes · E. Chinarro · F. M. Figueiredo (✉) · F. M. B. Marques · J. R. Frade
Department of Ceramics and Glass Engineering, CICECO, University of Aveiro, 3810-193 Aveiro, Portugal
e-mail: framos@cv.ua.pt

R. O. Fuentes
CINSO-CITEFA-CONICET, J.B. de la Salle 4397, B1603ALO Villa Martelli, Buenos Aires, Argentina

F. M. Figueiredo
Science and Technology Dep., Universidade Aberta, R. da Escola Politécnica 147, 1269-001 Lisbon, Portugal

R. Soares
Laboratório Central de Análises, University of Aveiro, 3810-193 Aveiro, Portugal

Introduction

A significant increase in both the ionic and electronic conductivities of $CaTiO_3$ is obtained upon substitution of Ti^{4+} by Fe^{3+} leading to the formation of oxygen vacancies and injection of electrons, at low oxygen partial pressure, and electron holes (coupled to the existence of Fe^{4+}), in oxidising conditions [1–3]. The maximum ionic conductivity is attained for 20 mol.% iron substitution [1–4] because tetra-coordinated trivalent iron is stabilised leading to oxygen vacancy ordering when the fraction of Fe exceeds this value [4, 5]. Thus, the composition $CaTi_{0.8}Fe_{0.2}O_{3-\delta}$ presents interesting levels of ambipolar transport and has been suggested for application as dense ceramic membrane for oxygen separation [1, 6, 7].

Materials usually obtained by conventional ceramic routes have a tendency to yield agglomerated powders with compositional inhomogeneities, and demand for relatively high sintering temperatures (≥1,320 °C for $CaTi_{0.8}Fe_{0.2}O_{3-\delta}$ [1–3,5–7]) in order to obtain dense ceramics. As for $BaTiO_3$-based materials [8], core-shell grains tend to develop in $CaTi_{0.8}Fe_{0.2}O_{3-\delta}$, with the grain interior consisting of pure $CaTiO_3$ and the periphery of an iron-substituted phase [9]. This is particularly evident for samples sintered for relatively short periods of time, c.a. 10 h at 1,320 °C, while still apparent for annealing times as large as 40 h. Although the presence of such inhomogeneities does not seem to

decrease performance [9], it certainly introduces an additional uncontrolled feature.

On the other hand, the interest for nanosized ceramics has been increasing as they may present properties different from those of materials with grain sizes in the micron range. However, the fabrication of bulk ceramics suitable for electrical conductivity (electronic and ionic) measurements is not an easy task and very few materials have been actually tested. Alternative processing methods yielding fine and reactive powders that demand lower sintering temperature include sol–gel, co-precipitation, hydrothermal reactions, citrate or nitrate routes and the mechanochemical synthesis in high-energy mills. The latter process has been successfully used to synthesize pure nano-crystalline $CaTiO_3$ powders [10, 11]. However, harsh milling conditions (about 700 rpm in a planetary ball mill) may lead to significant levels of contamination from the grinding media. A simpler approach consists on the mechanical activation of the precursors under milder milling conditions that, in principle, should considerably reduce the risk of contamination. The precursors, brought away from thermodynamic equilibrium (usually becoming amorphous) by the grinding energy, can then be heat treated to obtain the desired phase at a considerably lower temperature than that needed in a conventional ceramic route. Mechanical activation has been successfully applied to reduce the annealing temperature in the formation of strontium oxoferrates [12], lithium ferrites [13], strontium titanate [14, 15] and pure calcium titanate [16].

This article reports on the effects of the mechanical activation of TiO_2, Fe_2O_3 and $CaCO_3$ precursors aiming to obtain homogeneous $CaTi_{0.8}Fe_{0.2}O_{3-\delta}$ dense bulk ceramics with submicrometric grain size.

Experimental procedures

High purity powders of anatase TiO_2 (Merck), Fe_2O_3 (Riedel-de-Haën) and $CaCO_3$ (Merck), in the stoichiometric quantities, were mixed in ethanol in a ball mill during 2 h at 20 rpm and dried in air at 60 °C. The precursor mixtures were then activated at room temperature by dry grinding in planetary ball mills. Two experimental set-ups were used, one aiming to keep a low contamination level, and another where high milling energies were achieved. In the first the reactants were milled in a 100 cm^3 Teflon® container using a Restch PM 400 planetary ball mill operated at moderate velocities of 200 rpm and 300 rpm. In the second, a tetragonal stabilised zirconia (TZP) container (45 cm^3) was used in a Philips Mini Mill PW 4018/00 planetary ball mill operated at a constant 500 rpm. For both experiments, TZP balls (8 mm in diameter) were used as grinding media with a ball to powder weight ratio of 10:1. The grinding was interrupted at every 20 min to remove the powder from the wall of the containers.

The activated powders were analysed by X-ray diffraction (XRD) using a Rigaku Geigerflex diffractometer (CuK_α radiation, step 0.01°, 5 s/step) in order to identify compositional changes during grinding. The powder mixtures were also analysed in situ at high temperature by XRD (HTXRD) using an X'Pert MPD Philips diffractometer (CuK_α, step 0.01°, 5 s/step) equipped with a high temperature chamber, Anton-Parr GmbH HTK16, containing a Pt heating filament and a Pt–Pt/Rh(10%) thermocouple. The spectra were collected by the step counting method (step 0.05° and time 1 s) in the range 2θ = 10–40° at several temperatures with a heating rate of 10 K/min. The thermogravimetric (TGA) and differential thermal (DTA) analyses of the powders were carried out simultaneously with a constant heating rate of 5 K/min in a SETARAM TG-DTA LabSys instrument. The specific surface area was measured using a nitrogen adsorption Micromeritics Gemini 2370 BET surface area analyser, based on the Brunauer-Emmitt-Teller method (BET). The microstructure of the powders was evaluated by scanning (SEM) and transmission electron (TEM) microscopy using Hitachi S4100 SEM and 300 kV Hitachi H-9000 TEM microscopes, both equipped with Rontec energy dispersive X-ray spectroscopy (EDS) detectors that were used to assess the chemical inhomogeneity of the samples. The powders were dispersed in ethanol and placed in a biological glass sample holder for SEM analysis, or in a perforated Cu grid for TEM. Several selected area electron diffraction (SAED) patterns were collected.

Ceramic samples were obtained from powders isostatically pressed at 200 MPa and sintered in air. The sintering behaviour of green compacts was followed in air from 25 to 1,100 °C using an alumina Linseis dilatometer, with a heating rate of 5 K/min. The grain size and general microstructural features of these ceramics were analysed by SEM and TEM.

Results and discussion

Mechanical activation of $CaCO_3$-TiO_2-Fe_2O_3 mixtures

Figure 1 shows powder XRD patterns collected at different milling times and different rotation velocities.

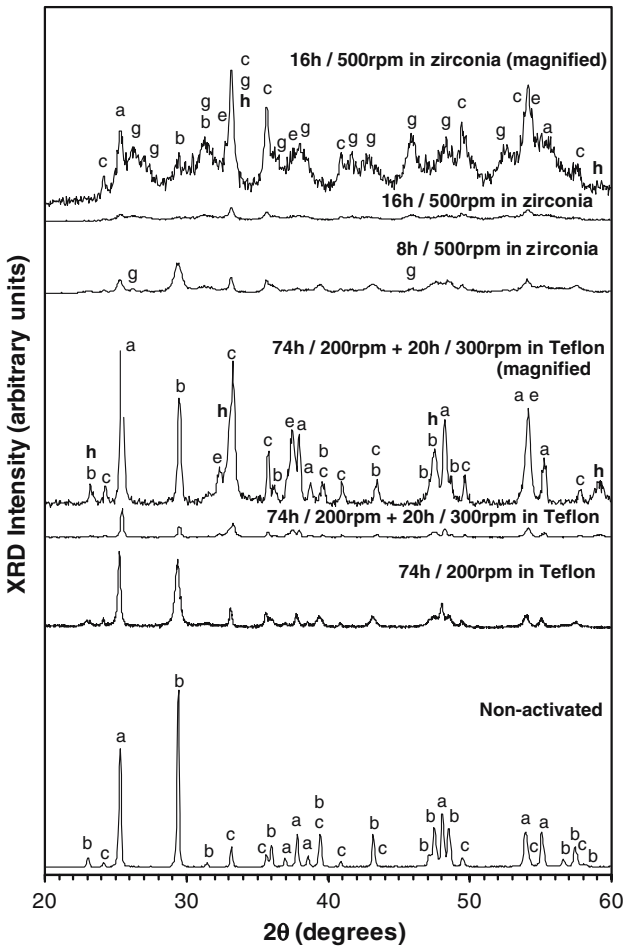

Fig. 1 XRD patterns of powders activated at 200 and 300 rpm in Teflon containers and at 500 rpm in zirconia containers for different periods of times. The peaks are indexed with letters corresponding to: (**a**) TiO_2 (anatase) (JCPDS-ICDD file no. 78-2486); (**b**) $CaCO_3$ (calcite) (JCPDS-ICDD file no. 88-1807); (**c**) Fe_2O_3 (JCPDS-ICDD file no. 89-0599); (**e**) CaO (JCPDS-ICDD file no. 82-1691); (**g**) $CaCO_3$ (aragonite) (JCPDS-ICDD file no. 76-0606); (**h**) $CaTiO_3$-like (JCPDS-ICDD file no. 82-0228)

It can be seen that for the powders activated in Teflon containers the intensity of the diffraction maxima decreases moderately with increasing milling time, when the velocity is kept at 200 rpm. The three reactants behave differently, with the intensity of the most important peak of $CaCO_3$ decreasing about 65% after 74 h (b peaks in Fig. 1), that from anatase about 35% (a peaks), and that of the hematite only about 10% (c peaks). Such differences are likely to be related to the hardness of each precursor. The Mohs hardness of calcite is 3 while that of anatase is about 5.5 and that of hematite is in the range 5.5–6.5. Thus, the effect of milling is expected to be more pronounced for calcite than for anatase and hematite. In the same experimental set-up, the increase to 300 rpm lead, after 20 h, to a significant decrease of the intensity of the TiO_2 and $CaCO_3$ peaks. In the latter case possibly also due to decarbonation since CaO diffraction maxima (e peaks) and possibly also to the formation of a perovskite phase, as suggested by the h peaks. The effect on the hematite peaks is weak and may indicate that the perovskite formed is nearly pure $CaTiO_3$. This phase was obtained from CaO and anatase after milling for 116 h at 200 rpm [11]. The fact that $CaCO_3$, instead of CaO, and the harder Fe_2O_3 were used in the initial mixtures might explain the differences. One may note that an alternative Fe precursor such as goethite (α-FeOOH) precursor may favour reaction, not only because it is slightly softer than hematite (5 Mosh) but because it is thermodynamically less stable [17, 18].

The energy input achieved by milling at 500 rpm in zirconia containers yields, as expected, a more significant decrease in the XRD peaks intensity for much shorter milling times. Moreover, the transformation of the calcite into the aragonite polymorph is apparent after milling for 8 h (g peaks). Although not detected in the present XRD analysis, the formation of vaterite, the least stable $CaCO_3$ polymorph, may also occur [19].

The effect of milling on microstructure is illustrated by the series of SEM micrographs shown in Fig. 2. The grain size of the initial powders is close to 250 nm (Fig. 2b), with calcite appearing in the form of large agglomerates with typical sizes in the range 5–15 μm (Fig. 2a). Milling at moderate rotation velocities (Fig. 2c) decreases the grain size to values smaller than 100 nm. The microstructure of the mixtures activated at 500 rpm is quite different. It consists of apparently larger agglomerates in which needle-like crystals are discernable (Fig. 2d). The acicular form of these crystals suggests that they are aragonite, in agreement with the XRD pattern shown in Fig. 1. The conversion of calcite to aragonite by mechanochemical action has been previously reported [19].

The TEM image presented in Fig. 3a indicates that the agglomerates in the mixture activated at 200 rpm consist of 25–50 nm particles. The corresponding electron diffraction pattern (Fig. 3b) shows dispersed, well defined spots, indicative of an essentially polycrystalline mixture since the diffuse rings, typical of the amorphous phases, are not present. Nevertheless, the presence of small fractions of amorphous material should not be completely ruled out. The dark field image (Fig. 3c) reveals crystals in light tonalities that are homogeneously distributed in the agglomerate. Figure 3d depicts another dark field image but from powders activated at 500 rpm. It can be seen that the particle size is fairly smaller. It can also be seen that the needle-shaped particles, ascribed to aragonite

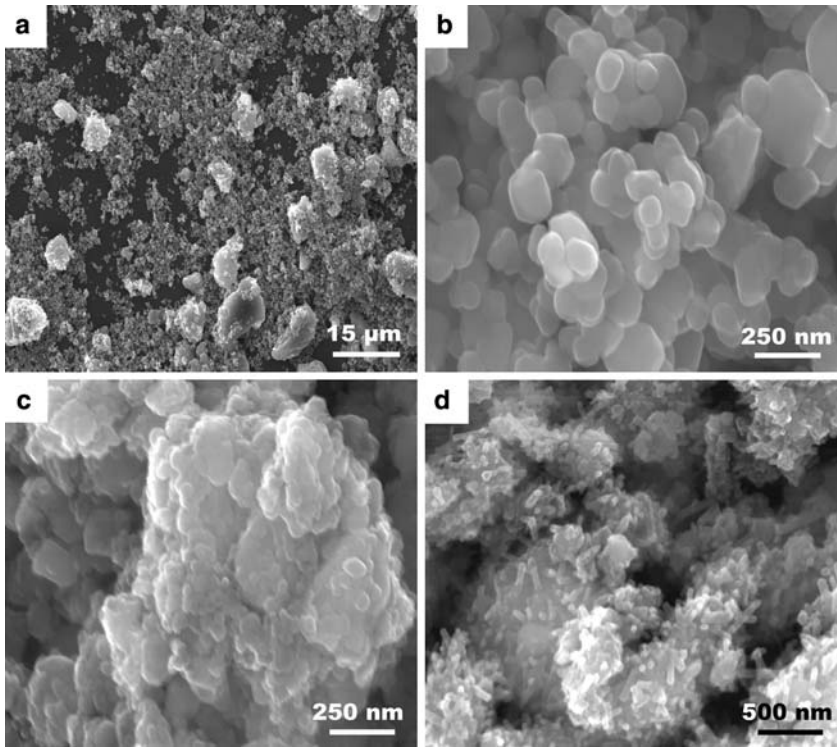

Fig. 2 SEM micrographs of the non-activated precursors (**a** and **b**), and activated at 200 rpm for 74 h followed by 20 h at 300 rpm in Teflon containers (**c**) and activated for 16 h at 500 rpm in zirconia containers (**d**)

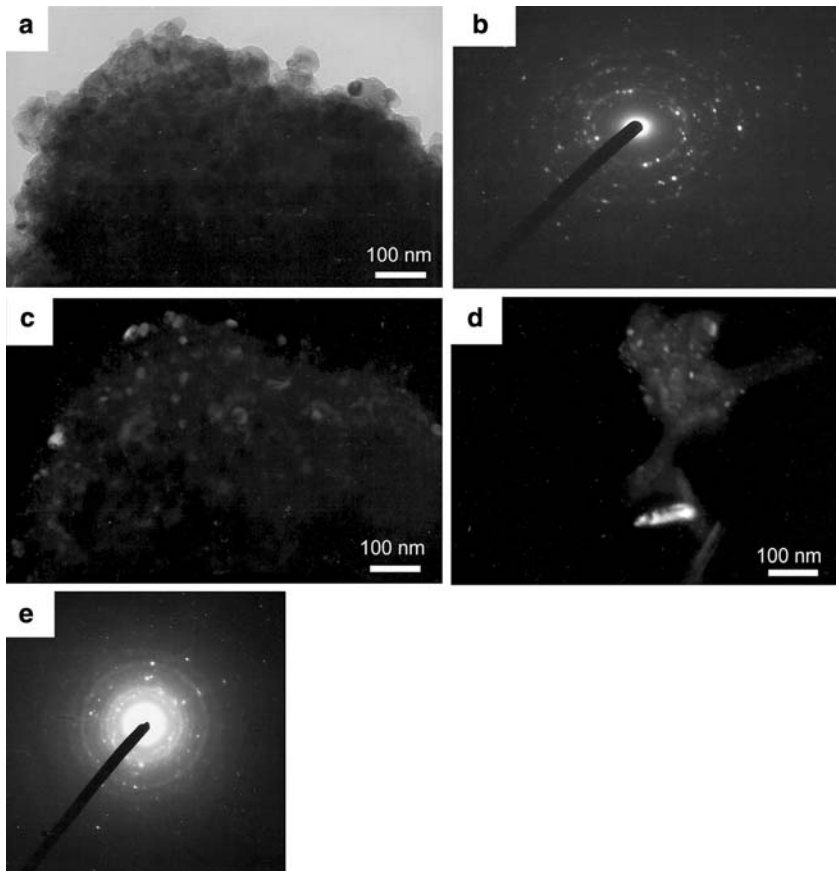

Fig. 3 TEM results obtained for powders activated at 200 rpm for 74 h plus 20 h at 300 rpm (bright (**a**) and dark (**c**) field images and corresponding SAED (**b**)) and at 500 rpm for 16 h (dark field (**d**) and SAED (**e**))

according to XRD (Fig. 1), are indeed crystalline. However, the electron diffraction pattern (Fig. 3e) depicts diffuse rings that suggest the existence of a significant fraction of amorphous material. This is an essential difference with respect to the non-activated mixtures and to those activated at low velocities.

High temperature treatments

The effect of the heat treatment on the phase composition of the mixtures activated at low velocities is illustrated by the in situ high temperature XRD results shown in Fig. 4. The 400 °C pattern shows that the CaO reacts with atmospheric CO_2 forming calcite, which eventually decomposes upon further heating at 900 °C. The availability of CaO enables the beginning of formation of the perovskite, in agreement with previous work [16]. Up to 900 °C, the intensity of the hematite peaks remains nearly unchanged, suggesting that the observed perovskite peaks should be due mainly to $CaTiO_3$. As expected, the increase in temperature facilitates the reaction and the diffraction maxima of the perovskite are predominant in the 1,200 °C pattern. However, hematite and a secondary perovskite phase, with a smaller lattice volume (left shoulders to the h peaks), are still present in non-negligible quantities. This secondary perovskite phase is likely to be $CaTiO_3$ because the substitution of Ti by Fe in $CaTiO_3$ leads to the lattice expansion [7, 20, 21] and, therefore, shifts the perovskite peaks to higher diffraction angles. Moreover, the perovskite main peaks in the 1,200 °C XRD pattern may be indexed only with a cubic lattice (space group $Pm\bar{3}m$), which is expected for $CaTi_{0.8}Fe_{0.2}O_{3-\delta}$ at $T \geq 940$ °C [20] but not for $CaTiO_3$, as in this case the transition to the cubic phase should occur at 1,250 °C [21]. One may thus suggest that the final product $CaTi_{0.8}Fe_{0.2}O_{3-\delta}$ forms via reaction of a $CaTiO_3$ intermediate with iron oxide. The formation of the Fe-containing perovskite could be facilitated by using an alternative, less stable Fe precursor such as goethite.

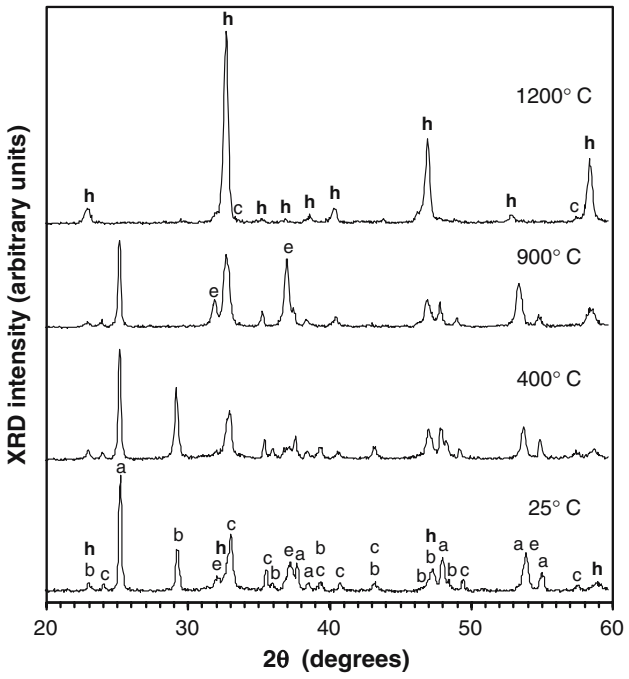

Fig. 4 XRD patterns obtained in situ at high temperature of precursors activated for 74 h at 200 rpm plus 20 h at 300 rpm. The peaks are indexed with letters corresponding to: (**a**) TiO_2 (anatase) (JCPDS-ICDD file no. 78-2486); (**b**) $CaCO_3$ (calcite) (JCPDS-ICDD file no. 88-1807); (**c**) Fe_2O_3 (JCPDS-ICDD file no. 89-0599); (**e**) CaO (JCPDS-ICDD file no. 82-1691); (**h**) 25 °C pattern indexed according $CaTiO_3$-like (JCPDS-ICDD file no. 82-0228), 1,200 °C pattern indexed with cubic $Pm\bar{3}m$ according to [16]

It should be noticed that for non-activated precursors the single perovskite material can only be obtained at temperatures higher than 1,250 °C and over considerably larger periods of time (>20 h) [9]. If the benefits from mild activation conditions are, therefore, moderate, clear differences can be observed in the XRD results depicted in Fig. 5, for the precursors activated at 500 rpm. The patterns collected at 450 and 300 °C indicate the temperature range where aragonite transforms into calcite, in agreement with previous observations [22]. More importantly, the perovskite peaks are already apparent in the 620 °C pattern and clearly dominate at 800 °C, although traces of anatase, calcia and hematite are still present. The pattern collected at 1,000 °C is that of a single cubic perovskite phase. This result suggests that although CaO availability is still the limiting factor to the perovskite formation, alternative reaction mechanisms involving titania and the less stable $CaCO_3$ polymorphs (aragonite) may be available when the precursors are mechanically activated.

Significant differences are also revealed by TGA/DTA analyses (Fig. 6). The curve for the non-activated mixture shows only one endothermic peak spanning from about 620 °C to 810 °C, coupled to a significant weight loss (Fig. 6a), certainly due to calcite decomposition. In the mixtures milled at low revolutions (74 h at 200 rpm plus 20 h at 300 rpm), the results show a slight decrease of the decarbonation temperature (about 10 °C less), which might be seen as an indication of the presence of aragonite or of amorphous $CaCO_3$ (and, possibly, also vaterite) formed during milling. The small endothermic peak at ca. 330 °C, associated to 3 wt.% loss, may correspond to the thermal decomposition of polytetrafluoroethylene, thus suggesting that contamination from Teflon pots

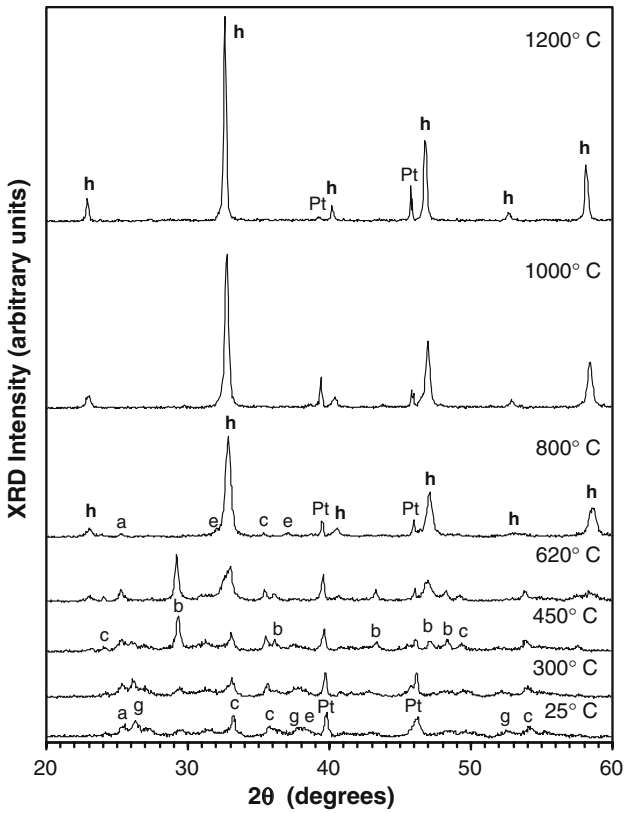

Fig. 5 XRD patterns obtained in situ at high temperature of the precursors activated for 16 h at 500 rpm. The peaks are indexed with letters corresponding to: (**a**) TiO_2 (anatase) (JCPDS-ICDD file no. 78-2486); (**b**) $CaCO_3$ (calcite) (JCPDS-ICDD file no. 88-1807); (**c**) Fe_2O_3 (JCPDS-ICDD file no. 89-0599); (**e**) CaO (JCPDS-ICDD file no. 82-1691); (**g**) $CaCO_3$ (aragonite) (JCPDS-ICDD file no. 76-0606); (**h**) 25 °C pattern indexed according $CaTiO_3$-like (JCPDS-ICDD file no. 82-0228), 1,200 °C pattern indexed with cubic *Pm*3*m* according to [16]

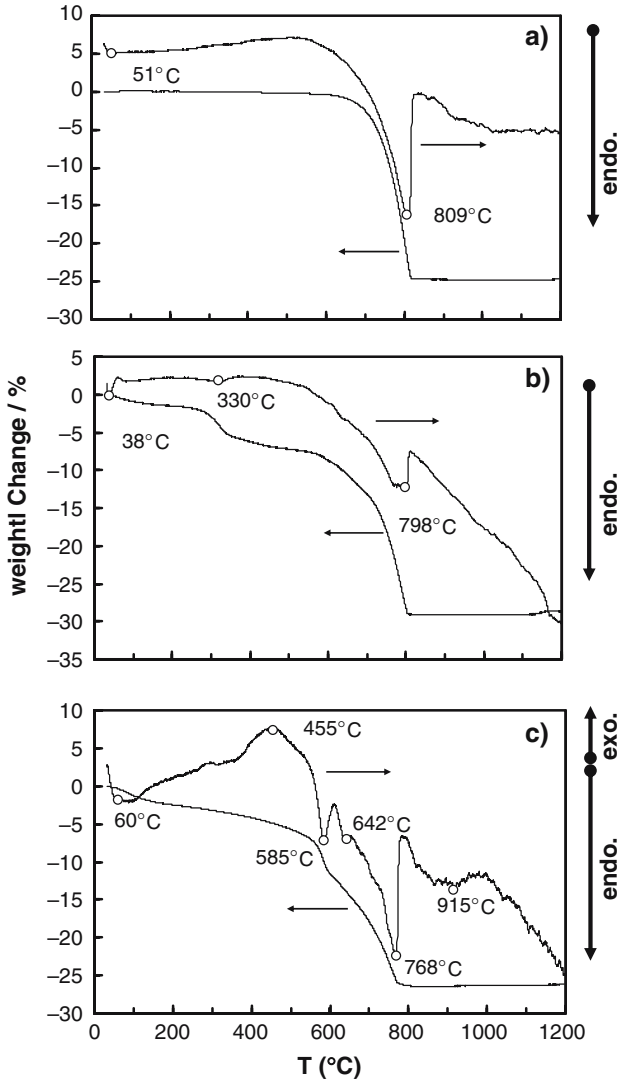

Fig. 6 Thermogravimetric and differential thermal analysis of (**a**) non-activated and powders activated for (**b**) 74 h at 200 rpm followed by 20 h at 300 rpm and (**c**) powders activated at 500 rpm for 16 h

occurs during milling. Note that since the formation of $CaCO_3$ from reaction of CaO with CO_2 (exothermic, leading to an increase of weight) should also occur in this temperature range (Fig. 4), the fraction of $CaCO_3$ decomposed during milling was probably very low. Therefore, it is a reasonable assumption that most of the calcite is not decomposed during milling, but rather brought to an amorphous state, possibly undergoing phase transitions to aragonite or vaterite intermediates. Indeed, the DTA curve obtained for the mixture activated at 500 rpm (Fig. 6c) shows a broad exothermic maximum at 430–460 °C that can be ascribed to the vaterite → calcite phase transition [17]. However, since only aragonite was detected by XRD (Fig. 1), this peak could instead be attributed to the crystallisation of calcite from amorphous $CaCO_3$. The endothermic phenomenon apparent at 585 °C, which has associated a weight loss, may be ascribed to the formation of the perovskite phase, noticed in the XRD pattern collected at 620 °C (Fig. 5), directly from the reaction of TiO_2 with a small fraction of aragonite that was not transformed into calcite. The endothermic reaction of the decomposition of calcite into CaO and CO_2 or/and the reaction of calcite with titanate ($CaCO_3$+TiO_2 → $CaTiO_3$+CO_2), spans from 650 °C to 770 °C, after which, as suggested by the XRD results in Fig. 5, the perovskite is the predominant crystalline phase. Note that the endothermic peak at 330 °C, ascribed to Teflon decomposition, is absent in this case, where the containers are made of zirconia.

Ceramics processing

Figure 7 depicts dilatometric curves for two green compacts of mechanically activated powders. The

behaviour is quite similar in both cases, with exception of minor differences in the temperature range below 400 °C, due to the effects of the release of adsorbed water (slight contraction at ca. 100 °C in both curves) and of the decomposition of Teflon-based contamination (contraction at 300 °C observed in curve A). These results are in agreement with the DTA/TGA results described above (Fig. 6). The dominating feature in both curves is the significant expansion observed up to about 700 °C, due to decomposition of calcium carbonate, after which densification takes place to be complete at ca. 900 °C. The temperature range over which the decarbonation occurs is broadened by the activation of the precursors at 500 rpm (curve B) and, consequently, the overall dimensional variation is smaller. The mechanical activation of the precursors is thus expected to favour sintering without previous calcination steps.

Nearly full dense ceramic samples (Fig. 8) were obtained after sintering at 1,125 °C or 1,150 °C for 2 h with intermediate temperature dwells of 1 h at 300 °C and 700 °C; the heating rate was 2 K/min at all stages. The temperature dwells and low heating rate facilitate the release of the gaseous species resulting from the decomposition of the polytetrafluoroethylene and, especially, the carbonate. The gas release leads to a significant dimensional variation (Fig. 7) that stresses the sample. Thus, the temperature dwells are essential to relax that stress and, therefore, to reduce the risks of cracking or even fracture. As both activated samples were sintered simultaneously, the sintering curve included the 300 °C dwell, in principle not needed for the samples activated in zirconia containers. The maximum temperature attained in this sintering cycle is about 200 °C lower than that used to obtain dense ceramics from non-activated precursors [1, 2, 9]. The direct consequence of such low densification temperature is the possibility to retain, in the ceramics, the small grain size of the initial powders. Figure 8 reveals clear submicrometric microstructures with a bimodal grain size distribution. No secondary phases were detected, in agreement with Fig. 5. The smaller grains have an equivalent diameter ca. 100 nm while in the larger ones, probably originated from the agglomerates, it is of the order of 250 nm for the samples activated at 200 and 300 rpm, and of 500–700 nm for the 500 rpm sample. Such difference in the size of the larger grains is probably due to the larger agglomerates apparent in the latter case (Fig. 2c, d). The grain size reported for ceramics obtained from non-activated samples sintered at 1,320–1,350 °C for 2 h is close to 3 μm or greater [1, 6, 9]. Moreover, in these samples, the chemical and microstructural homogeneity attained under such processing conditions is rather low with TEM revealing the presence of a large fraction of

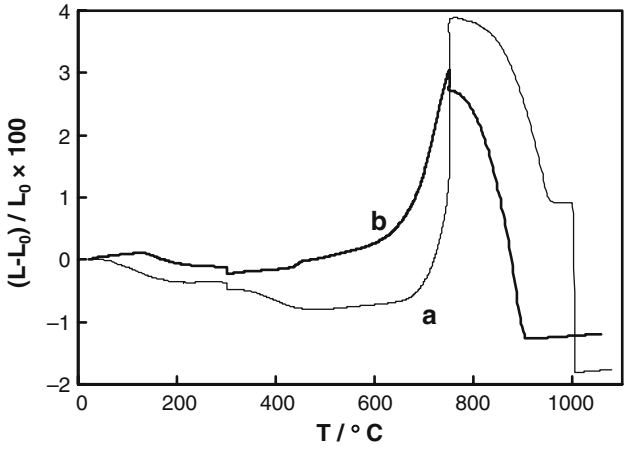

Fig. 7 Dimensional variations for uniaxially pressed powders heated at 5 K/min: (**a**) mixtures activated for 74 h at 200 rpm plus 20 h at 300 rpm; (**b**) mixtures activated for 16 h at 500 rpm

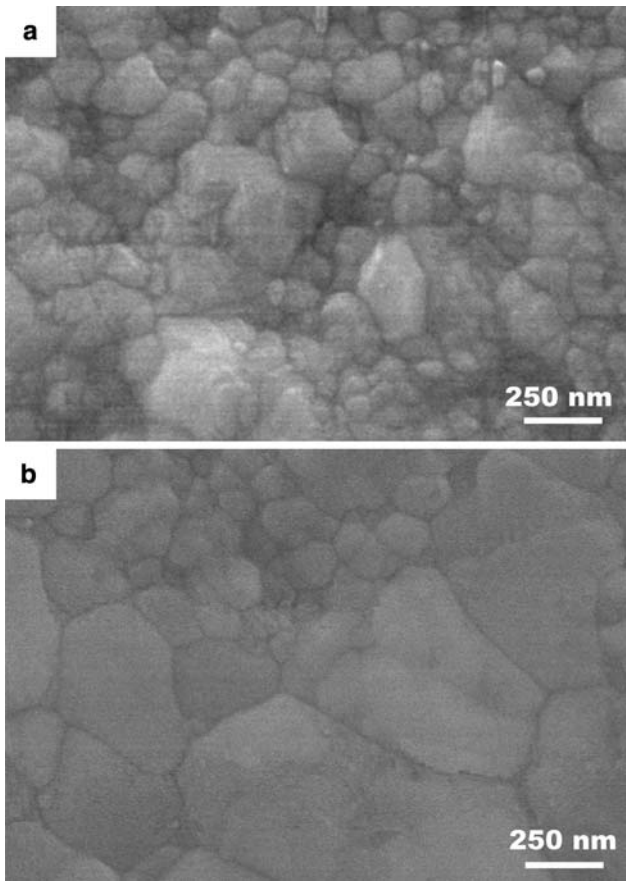

Fig. 8 SEM micrographs of $CaTi_{0.8}Fe_{0.2}O_{3-\delta}$ ceramics obtained from powders activated for (**a**) 74 h at 200 rpm plus 20 h at 300 rpm and sintered at 1,150 °C for 2 h, and for (**b**) 16 h at 500 rpm sintered at 1,125 °C for 2 h

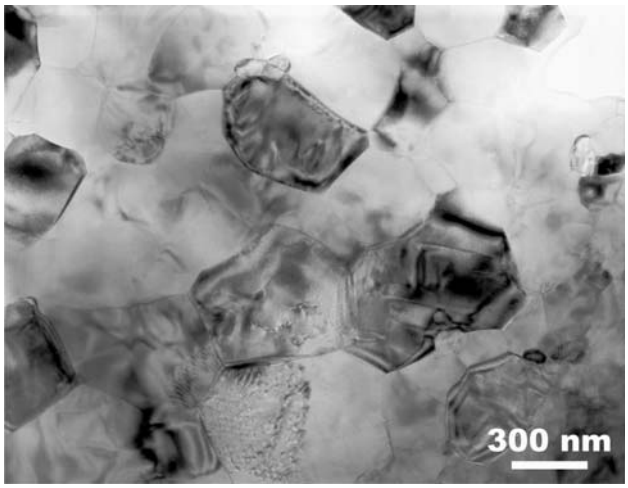

Fig. 9 TEM micrograph of a $CaTi_{0.8}Fe_{0.2}O_{3-\delta}$ ceramic obtained from powders activated for 16 h at 500 rpm and sintered at 1,125 °C for 2 h

grains with core-shell structure; a core consisting of pure $CaTiO_3$ surrounded by a Fe-containing shell [9]. It has been further shown that significantly larger annealing times (of the order of 40 h) are necessary to obtain ceramics free from core-shell grains. For the activated samples described in this work, however, core-shell inhomogeneities could not be detected (Fig. 9) and no cation segregation could be detected by TEM/EDS.

Conclusions

The processing of $CaTi_{0.8}Fe_{0.2}O_{3-\delta}$ dense ceramics by the traditional ceramic route is significantly facilitated by mechanical activation of the precursors. Single-phase materials can be obtained after calcining at temperatures as low as 1,000 °C. The advantages over the classical ceramic route appear to be related to a significant improvement of the reaction kinetics, due to the smaller grain size (<100 nm) of the activated powders, and also to a modification of the initial thermodynamic state of the reactants, associated to the transition to an amorphous state or to metastable polymorphs such as aragonite.

The advantage of using mechanically activated precursors to obtain dense homogeneous ceramic samples is clearly demonstrated by a decrease of about 200 °C in the maximum sintering temperature, in comparison to non-activated samples, typically sintered at 1,320–1,350 °C. These ceramics partially retain the fine microstructure of the initial powders, showing a bimodal grain-size distribution with grain sizes in the range 100–200 nm and 250–500 nm for small and large grains, respectively.

Acknowledgements This work was supported by the FCT (POCI/CTM/59727/2004), Portugal. E. Chinarro was awarded a Marie Curie fellowship of the European Community Programme IHP under contract number HPMT-CT-2000-00206.

References

1. Esaka T, Fujii T, Suwa K, Iwahara H (1990) Solid State Ionics 40/41:544
2. Sujita D, Norby T, Osborg PA, Kofstad P (1993) In: Singhal SC, Iwahara H (eds) Proc. of the 3rd Int. Symposium on Solid Oxide Fuel Cells, Electrochem. Soc. Proc., vol 93–4. Electrochemical Society, Pennington, NJ, pp 552–561
3. Selçuk A, Steele BCH (1995) Fourth Euro Ceramics-vol 5, Gusmano G, Traversa E (eds) (Editoriale Faenza Editrice S.p.A. 413)
4. Figueiredo FM, Waerenborgh JC, Kharton VV, Näffe H, Frade JR (2003) Solid State Ionics 156:371
5. Grenier J-C, Schiffmacher G, Caro P, Pouchard M, Hagenmuller P (1977) J Solid State Chem 20:365
6. Itoh H, Asano H, Fukuroi K, Nagata M, Iwahara H (1997) J Am Ceram Soc 80(6):1359
7. Figueiredo FM, Soares MR, Kharton VV, Naumovich EN, Waerenborgh JC, Frade JR (2004) J Electroceramics 13:627
8. Hennings D, Rosenstein G (1984) J Am Ceram Soc 67(4):249
9. Figueiredo FM, Kharton VV, Waerenborgh JC, Viskup AP, Naumovich EN, Frade JR (2004) J Am Ceram Soc 87(12):2252
10. Mi G, Saito F, Suzuki S, Waseda Y (1998) Powder Technol 97(2):178
11. Berry FJ, Wynn P, Jiang J, Mørup S (2001) J Mat Sci 36:3637
12. Berbenni V, Marini A (2002) Mat Res Bull 37:221
13. Berbenni V, Marini A, Matteazzi P, Ricceri R, Welham NJ (2003) J Eur Ceram Soc 23:527
14. Wang J, Yin S, Zhang Q, Saito F, Sato T (2003) J Mater Chem 13:2348
15. Hungría T, Hungría A-B, Castro A (2004) J Solid State Chem 177:1559
16. Evans IR, Howard JAK, Sreckovicb T, Risticc MM (2003) Mat Res Bull 38:1203
17. Stumm W, Morgan JJ (1981) Aquatic Chemistry. 2nd Edn, John Wiley & Sons, New York, 753
18. NBS Tables of Chemical Thermodynamic Properties (1982) J Phys Chem Ref Data, 11, Supplement 2, 1982
19. Thomas JM, Renshaw GD (1967) J Am Chem Soc 89A:2058
20. Becerro AI, Redfern SAT, Carpenter MA, Knight KS, Seifert F (2002) J Solid State Chem 167:459
21. Redfern SAT (1996) J Phys Condens Matter 8:8267
22. Petrić J, Vučak M, Krstulović R, Brečević Lj, Kralj D (1996) Thermochim Acta 277:175